Photonic Nanolaser with Extreme Optical Field Confinement

Hao Wu,[1] Liu Yang,[1] Peizhen Xu,[1] Jue Gong,[1] Xin Guo,[1,2,3,*] Pan Wang,[1,2,3] and Limin Tong[1,4,†]
[1]*Interdisciplinary Center for Quantum Information, State Key Laboratory of Modern Optical Instrumentation, College of Optical Science and Engineering, Zhejiang University, Hangzhou 310027, China*
[2]*Jiaxing Key Laboratory of Photonic Sensing and Intelligent Imaging, Jiaxing 314000, China*
[3]*Intelligent Optics and Photonics Research Center, Jiaxing Institute of Zhejiang University, Jiaxing 314000, China*
[4]*Collaborative Innovation Center of Extreme Optics, Shanxi University, Taiyuan 030006, China*

(Received 1 October 2021; accepted 23 May 2022; published 28 June 2022)

We proposed a photonic approach to a lasing mode supported by low-loss oscillation of polarized bound electrons in an active nano-slit-waveguide cavity, which circumvents the confinement-loss trade-off of nanoplasmonics, and offers an optical confinement down to sub-1-nm level with a peak-to-background ratio of ∼30 dB. Experimentally, the extremely confined lasing field is realized as the dominant peak of a TE_0-like lasing mode around 720-nm wavelength, in 1-nm-level width slit-waveguide cavities in coupled CdSe nanowire pairs. The measured lasing characteristics agree well with the theoretical calculations. Our results may pave a way towards new regions for nanolasers and light-matter interaction.

DOI: 10.1103/PhysRevLett.129.013902

Laser with tighter field confinement is a key to lower-dimensional light-matter interaction for applications ranging from optical microscopy, sensing, photolithography, to information technology [1–3]. Generally, limited by optical diffraction, a photonic lasing cavity is unable to confine fields much better than half the vacuum wavelength ($\lambda_0/2$) [2,4]. The emerging plasmonic nanocavity opens a route towards deep-sub-diffraction lasing field with optical confinement down to $\lambda_0/30$ [5–11]. However, due to the trade-off between optical confinement and plasmon loss of oscillating free electrons that is intrinsically originated from Landau damping in metals [12], scaling down the cavity size of a plasmon nanolaser is a great challenge due to the insufficient gain and thermal damage [4,10,13].

On the other hand, complying with the electromagnetic boundary conditions [14], tight field confinement (e.g., down to 10-nm level) has recently been demonstrated in photonic interfaces such as slot waveguides [15,16] and bowtie-shaped dielectric structures [17–20], indicating a possibility to surpass the field confinement of plasmonic nanostructures if the interface size can be further scaled down.

Here we propose a purely photonic approach to circumvent the confinement-loss trade-off and offer an extreme field confinement ($\sim\lambda_0/1000$). Based on a photonic nanocavity formed in a high-gain slit waveguide in a coupled nanowire pair (CNP), our calculations show that a low-threshold TE_0-like lasing mode in a 1-nm-slit CdSe CNP can offer a field confinement down to 0.29 nm and a peak-to-background ratio of about 30 dB, with much higher cavity-to-free-space emission efficiency. Experimentally, pumped by 532-nm-wavelength laser pulses, the TE_0-like lasing mode around 720-nm wavelength is observed in CdSe CNPs, with lasing characteristics agreeing well with theoretical calculations.

The configuration of the nanolaser is schematically illustrated in Fig. 1(a). The CNP, supported on a low-refractive-index substrate (e.g., a MgF_2 crystal with index of 1.38), is formed by a pair of identical high-gain semiconductor nanowires typically having a hexagonal cross section, a smooth surface (section I in Supplemental Material [21]) and a uniform diameter (defined as the diagonal of its hexagonal cross section). Relying on the coupled oscillation of polarized bound electrons around its both sides (section II in Supplemental Material [21]), the slit can support a hybrid TE_0-like waveguiding mode with a central hotspot in the cross section of the CNP [Fig. 1(b), see section III in the Supplemental Material [21]]. For quantitative calculation, we assume the nanowire material to be CdSe (refractive index n of 2.6 at 720-nm wavelength [36]), and calculate the modal profile of the TE_0-like mode using a finite element method with a linear transition of index (Fig. S2 in the Supplemental Material [21]). Since the optical response of the nanowire we investigated here is dominated by bound electrons, classical electromagnetic theory remains valid for simulating its photonic response with feature size well below 1 nm [37]. When the slit width is small enough (e.g., 1-nm scale), the TE_0-like mode at 720-nm wavelength (typical lasing wavelength of CdSe nanowires [38–40]) can offer a central peak at the hotspot with ultratight field confinement and large peak-to-background ratio (e.g., ∼30 dB, with definition given in section IV in the Supplemental Material [21]). Figures 1(c) and 1(d) give the calculated field confinement, defined as the full width at half maximum (FWHM) of the field intensity of the TE_0-like mode (the fundamental

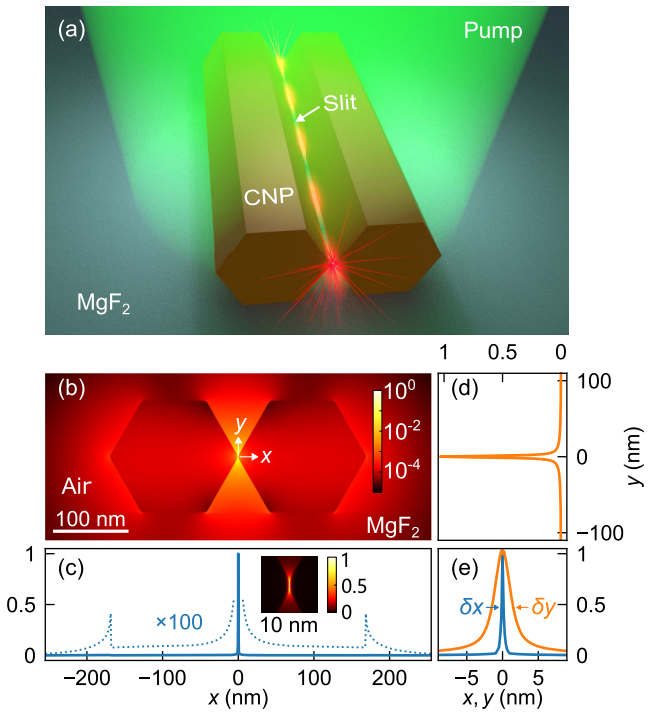

FIG. 1. CNP for extreme optical field confinement at 720-nm wavelength. (a) Schematic illustration of a CNP-based nanolaser. (b) Calculated cross-sectional electric field intensity of a TE_0-like mode in a CNP with nanowire diameter $d = 170$ nm and slit width $w = 1$ nm. (c),(d) Field intensity distribution along the horizontal (x axis) direction ($y = 0$) and the vertical (y axis) direction ($x = 0$) in (b), respectively. Inset: close-up of the field intensity around the slit in (b). For better clarity, a 100× profile is also plotted as dotted lines in (c). (e) Close-up view of the intensity profiles in (c) and (d).

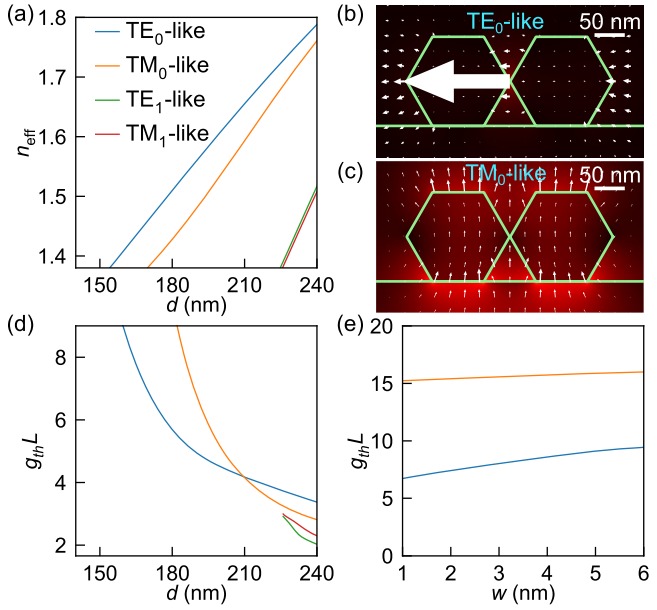

FIG. 2. Laser modeling of a CdSe CNP cavity at 720-nm wavelength. (a) The first 4 modes (TE_0-, TM_0-, TE_1-, and TM_1-like modes) supported in a CNP with $w = 1$ nm, and their calculated effective refractive indices n_{eff}. (b),(c) Electric field vectors of the TE_0- and TM_0-like modes with $d = 170$ and $w = 1$ nm. The orientation and size of the white arrow indicate the polarization and amplitude of the local field. (d),(e) Threshold gain $g_{\mathrm{th}}L$ of the first 4 modes with (d) $w = 1$ and (e) $d = 170$ nm, respectively.

waveguiding mode); the 0.29 (x axis) and 2.83-nm (y axis) spatial confinement offer a spot size down to $\sim 6.2 \times 10^{-6}\lambda_0^2$ [Fig. 1(e), see also Fig. S8(a)].

Apart from the central peak, the TE_0-like mode has a low-intensity background field that is largely flat inside the CdSe nanowire and faded out quickly beyond the nanowire's farmost edges [dotted line in Fig. 1(c)]. Unlike a plasmonic mode that is wholly subdiffraction confined, here the TE_0-like mode as a whole is diffraction limited. However, the subnanometer-level low-loss optical field confinement is far beyond the reach of a plasmonic mode (see section V in the Supplemental Material [21]). A certain background field is critical to bestow the central peak with high intensity and slow decay outside the end face while maintaining an extreme optical confinement. Also, when interfacing with free-space photons, the momentum mismatch of this photonic mode is much smaller than that of an ultraconfined plasmonic mode.

Meanwhile, within a ~0.0043% of the total mode area, the ultraconfined central peak concentrates ~0.11% of the total mode power (section VI in the Supplemental Material [21]). Calculated fraction of the mode power contained inside the CdSe nanowire is ~37.1%, contributing to a confinement factor Γ_g of ~0.52 for the CNP (section VII in the Supplemental Material [21]), which is favorable for reducing the lasing threshold [41].

To explore the lasing modes in the CNP, we first calculate its guiding modes at 720-nm wavelength with a slit width w of 1 nm. When the nanowire diameter d is less than 225 nm, the CNP supports only TE_0- and TM_0-like modes [Fig. 2(a) and section VIII in the Supplemental Material [21]]. The TE_0-like mode is nearly horizontally polarized [Fig. 2(b)], while the TM_0-like mode is basically vertically polarized [Fig. 2(c)].

In a Fabry-Perot-type CNP cavity, the lasing threshold gain g_{th} provided by the nanowire can be obtained as $g_{\mathrm{th}}L = 1/\Gamma_g \ln(1/R)$ [42], where L is the nanowire length and R the single-trip reflectivity (see section VII in the Supplemental Material [21]). Calculated $g_{\mathrm{th}}L$ [Figs. 2(d) and 2(e)] shows that, lasing thresholds of both modes increase monotonically with decreasing d and increasing slit width w, which is reasonable as smaller d offers lower effective gain (less gain material) and higher round-trip loss (lower end face reflectivity), and increasing w decreases Γ_g. In particular, compared with the TM_0-like mode, the TE_0-like mode has a lower threshold with $d < 209$ nm when $w = 1$ nm [Fig. 2(d)], or at least $w < 6$ nm when

$d = 170$ nm [Fig. 2(e)]. In addition, the calculated quality factor (Q factor) of the TE_0-like mode of a CNP with 20-μm length and 170-nm nanowire diameter is ~60. Compared with Q factors reported in other semiconductor nanowires with larger diameters [39], this Q factor is relatively lower due to the lower end face reflectivity of a thinner nanowire, which could be enhanced by forming Bragg gratings at one side of the CNP.

Figure 3(a) shows the calculated near-field intensity evolution of the cavity mode emitting into free space. As it escapes out of the CNP end face, the field of the central peak spreads out with decreasing intensity [Fig. 3(b)], a similar behavior as light transmission through a deep-subwavelength aperture [43,44], and can be interpreted as an inevitable result of the Heisenberg uncertainty relation (section IX in the Supplemental Material [21]).

However, since the majority of the mode power is distributed in the diffraction-limited background field, the effective index of the TE_0-like mode (e.g., 1.46 with $d = 170$ nm) is not very large compared with that of light in free space [Fig. 2(a)], leading to an overall transmissivity, i.e., the ratio of overall transmitted power to the mode power inside the cavity, as high as 0.95 [Fig. 3(c)], much higher than that of a deep-subwavelength aperture with similar lateral field confinement [e.g., 4.10×10^{-16} for a 1-nm-diameter aperture, see Fig. 3(d)]. It is worth mentioning that a plasmonic background field was proved effective for momentum compensation with aperture size down to ~150 nm [45]. However, for a 1-nm aperture, the momentum mismatch is too large to be compensable in this way. Moreover, the relatively slow intensity decay of the output field outside the end face is particularly desirable for near-field light-matter interaction for nanoscale objects (Fig. S12 in the Supplemental Material [21]).

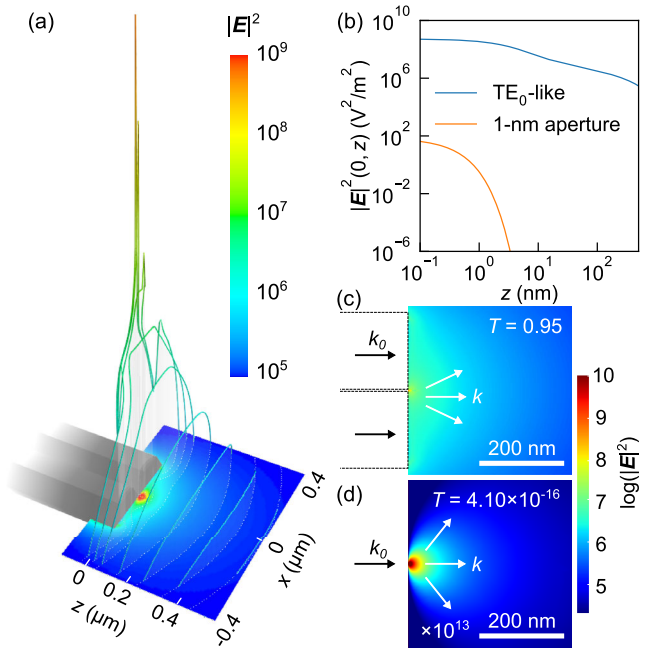

FIG. 3. Calculated near-field intensity evolution of optical field output from a TE_0-like mode in a CNP ($d = 170$ nm, $w = 1$ nm) and a circular aperture (1-nm diameter). (a) Evolution of $|\boldsymbol{E}|^2$ of the TE_0-like mode output from a CNP end face. A series of isophases of E_x are plotted for better visualization. (b) Evolution of $|\boldsymbol{E}|^2(0, z)$ of the field output from a TE_0-like mode (blue) and a 1-nm aperture (orange), respectively. (c),(d) $|\boldsymbol{E}|^2$ of an optical field with a wave vector of k_0 output from (c) a CNP end face and (d) a 1-nm aperture. The calculated overall transmissivity T is also presented. For better visualization, the intensity in (d) is amplified by a factor of 10^{13}. The input field is 720 nm in wavelength and 1 nW in power.

To experimentally realize such a nanolaser, we construct the CNP using single-crystal wurtzite CdSe nanowires synthesized via a physical vapor deposition method [46]. These nanowires typically have an atomic-level sidewall smoothness for low-loss waveguiding [47] and a gain high enough (e.g., $> 0.1\ \mu m^{-1}$ around 700-nm wavelength [48]) for supporting lasing oscillation in a short (e.g., 10-μm level) cavity [40]. Although our calculation has shown that a CNP supports only a TE_0-like mode when 154 nm $< d <$ 169 nm [Fig. 2(a)], experimentally nanowires with such small diameters have large substrate-induced leakage losses and lower effective gain, and thus higher lasing threshold [7,49], which requires a high pump density that is very likely to damage the CNP. Therefore, to facilitate the experimental realization, we prefer to use nanowires with larger diameters (i.e., 154 nm $< d <$ 209 nm, see Fig. 2(d)], with which the TE_0-like mode has a much lower threshold gain, and TE_0- and TM_0-like modes can be readily identified by their orthogonal polarizations.

As shown in Fig. 4(a), we assemble a CNP using two identical nanowires (cut from the same CdSe nanowire with $d = 166$ nm) in close contact in parallel via micromanipulation, and mill both ends of the CNP via focused ion beam to form a CNP with $L = 22.4\ \mu$m [Fig. 4(a), see also section X in the Supplemental Material [21]].

After milling, the CNPs typically have flat end faces [Fig. 4(b), see also section XI in the Supplemental Material [21]]. With a surface roughness of ~1 nm, the slit width between the two opposite nanowire vertex edges is about 1 nm [Fig. 4(c), see also Fig. S15] with a V-shaped linearly changing index profile [inset of Fig. 4(c), see also section I in the Supplemental Material [21]]. To pump the CNP, we loosely focus a beam of 532-nm-wavelength laser pulses (5-ns pulse width and 2-kHz repetition rate) onto the whole length of the CNP using an objective of relatively low numerical aperture (NA), and collect emission from the CNP end face via a high-NA objective [Fig. 4(d), see also section XII in the Supplemental Material [21]]. Under a low pump density, the output end face of the CNP is a dim red-color spot in optical micrograph [Fig. 4(e)]. When the pump density exceeds a certain threshold, the end face output abruptly goes brighter with clear interference fringes

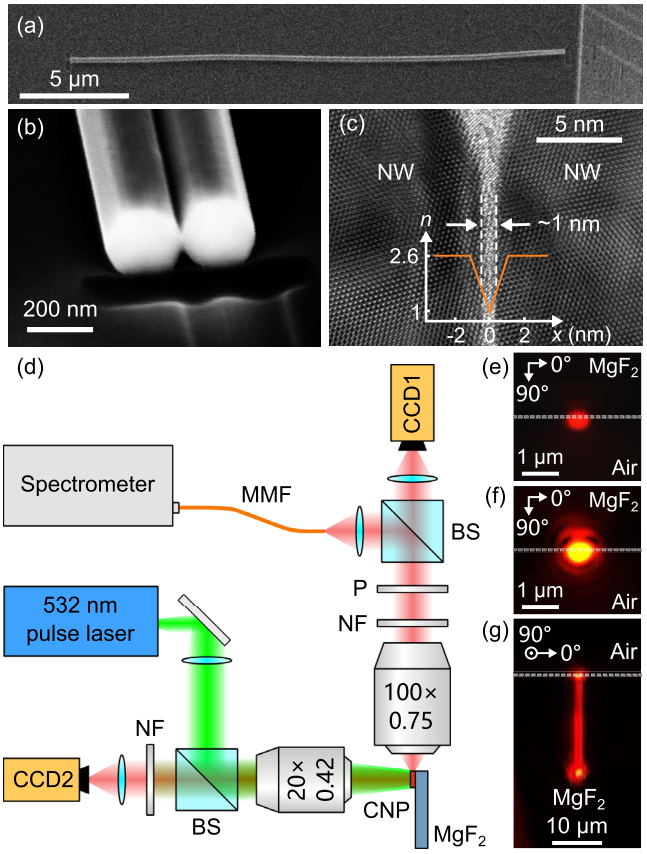

FIG. 4. Experimental realization of the CdSe CNP nanolaser. (a) Scanning electron microscopy (SEM) image of a CdSe CNP with $d = 166$ nm, $L = 22.4$ μm, and $w = 1$ nm. (b) SEM image of a flat end face of the CNP. (c) High-resolution transmission electron microscope image of the 1-nm-width slit. Inset: refractive-index profile around the slit. (d) Schematic of the experimental setup for lasing characterization. Multimode fiber (MMF); beam splitter (BS); polarizer (P); notch filter (NF). (e),(f) Optical images of the end face of CNP from CCD1 (e) below and (f) above the lasing threshold, respectively. (g) Optical image of the CNP from CCD2 around the lasing threshold. Dashed lines in (e)–(g) mark the edge of the substrate.

[Figs. 4(f) and 4(g)], confirming the higher intensity and better coherence of the emission above the lasing threshold.

Figure 5(a) shows the photoluminescence (PL) spectra collected from the end face of a typical CNP ($d = 158$ nm). When the pump density increases to 1.4 MW/cm^2, an evident peak at 709.2 nm emerges. Since the measured polarization of the peak is horizontal [inset of Fig. 5(a)] and d is smaller than the cutoff diameter of TE_1-like modes, the lasing mode is thus a TE_0-like mode, which is also predicted in Fig. 2(d). Figure 5(b) shows the pump-density-dependent output intensity and linewidth of the PL peak. The typical S curve of peak intensity under log-log scale shows the evolution from spontaneous emission to amplified spontaneous emission, and finally lasing oscillation at lasing threshold of 1.4 MW/cm^2, accompanying with evident linewidth narrowing from ~3 to 0.5 nm (measured with a resolution of 0.035 nm). Figure 5(b) also gives the measured degree of second-order coherence $g^{(2)}(0)$. When the pump density is increased from well below to approach the lasing threshold (1.4 MW/cm^2), $g^{(2)}(0)$ increases from ~1 (due to the averaging effect of detector [50]) to ~1.31, clearly showing the thermal bunching of the photons. When the pump density is further increased to exceed the threshold, $g^{(2)}(0)$ decreases to ~1, agreeing well with those observed in typical nanolasers [50,51], which confirms the lasing action in the CNP.

Since a direct measurement of a sub-1-nm field confinement is beyond the reach of current techniques, to obtain more evidences of the TE_0-like lasing mode, we have investigated a collection of CNP-based nanolasers with different d, and compared experimental results with theoretical calculations. Figure 5(c) summarizes the peak wavelength and polarization of the first-appeared (i.e., the lowest-threshold) lasing mode with respect to d (see also section XIII in the Supplemental Material [21]). For comparison, the calculated d-dependent polarization distribution of the lowest-threshold lasing modes is plotted as a three-region background: region I for TE_0-like modes with horizontal polarization, region II for TM_0-like modes with vertical polarization, and region III for TE_1-like modes with horizontal polarization. It shows that, with relatively small d, the first 4 modes (white solid triangles) are all horizontally polarized TE_0-like modes, falling well in the predicted region I. With increasing d, the next 5 modes (black hollow squares) are vertically polarized TM_0-like modes, largely agreeing with theoretical prediction. The slight deviation of the first mode ($d = 197$ nm) from region II may result from small errors of refractive index and measured d of the nanowire. When d exceeds the cutoff diameter of the TE_1-like modes, the last 4 modes are horizontally polarized TE_1-like modes, falling well in the predicted region III.

Overall, we have demonstrated a CNP-based photonic nanolaser with subnanometer-level field confinement. Compared with existing nanolasers, this laser can offer not only much tighter field confinement, but also much higher output efficiency, which may open an avenue for light-matter interaction on much lower dimensions, e.g., efficiently interfacing photons with single molecules or atoms with high spatial selectivity. In addition, the ultralarge field gradient of the central peak (see section XIV in the Supplemental Material [21]) is promising for subnanometer imaging [52], and atom or nanoparticle trapping [53]. Moreover, without the tunneling-induced quenching (e.g., in plasmonic nanogaps [54]), the slit width may be further scaled down by using nanowires with lower surface roughness to achieve tighter field confinement. With its unparalleled field confinement, the nanolaser shown here may inspire a new category of nanolasers and push the limit of laser-based science and technology beyond the nanometer scale.

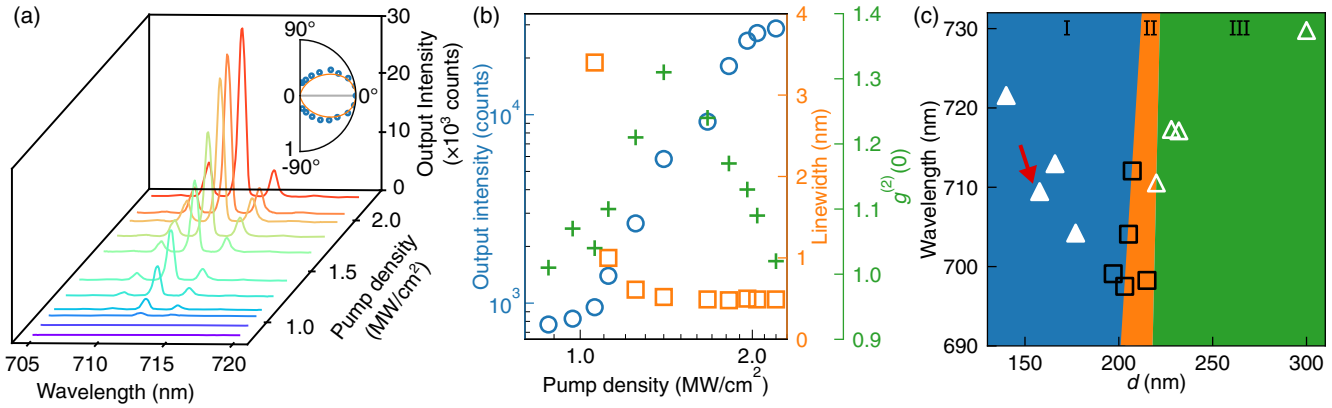

FIG. 5. Lasing characteristics of the CdSe CNPs. (a) Measured photoluminescence spectra obtained from the end face of a CNP ($d = 158$ nm). Inset: measured (blue circle) and calculated (orange line) polarization-dependent intensity of the peak with pump density of 2.2 MW/cm^2. (b) Pump-density-dependent output intensity (blue circle), linewidth (orange square), and degree of second-order coherence $g^{(2)}(0)$ (green cross) of the peak in (a). (c) Distribution of mode with the lowest threshold gain (I: TE_0-like; II: TM_0-like; III: TE_1-like) with varying d and lasing wavelength. Samples investigated with different d, lasing wavelength, and polarization (white triangle: horizontal polarization; black square: vertical polarization) are also marked. The sample employed in (a) and (b) is marked with a red arrow.

This work is supported by the National Key Research and Development Project of China (2018YFB2200404), the National Natural Science Foundation of China (61635009, 92150302, 62175213, and 11527901), the Natural Science Foundation of Zhejiang Province (LR21F050002), and the Fundamental Research Funds for the Central Universities. The authors thank Yixiao Gao for helpful discussion and Zhanke Zhou for help in lasing characterization.

H. W. and L. Y. contributed equally to this work.

*guoxin@zju.edu.cn
†phytong@zju.edu.cn

[1] P. Norvig *et al.*, 2020 visions, Nature (London) **463**, 26 (2010).
[2] M. T. Hill and M. C. Gather, Advances in small lasers, Nat. Photonics **8**, 908 (2014).
[3] R.-M. Ma and R. F. Oulton, Applications of nanolasers, Nat. Nanotechnol. **14**, 12 (2019).
[4] J. B. Khurgin and G. Sun, How small can "Nano" be in a "Nanolaser"?, Nanophotonics **1**, 3 (2012).
[5] D. J. Bergman and M. I. Stockman, Surface Plasmon Amplification by Stimulated Emission of Radiation: Quantum Generation of Coherent Surface Plasmons in Nanosystems, Phys. Rev. Lett. **90**, 027402 (2003).
[6] M. T. Hill, M. Marell, E. S. P. Leong, B. Smalbrugge, Y. Zhu, M. Sun, P. J. van Veldhoven, E. J. Geluk, F. Karouta, Y.-S. Oei, R. Nötzel, C.-Z. Ning, and M. K. Smit, Lasing in metal-insulator-metal sub-wavelength plasmonic waveguides, Opt. Express **17**, 11107 (2009).
[7] R. F. Oulton, V. J. Sorger, T. Zentgraf, R.-M. Ma, C. Gladden, L. Dai, G. Bartal, and X. Zhang, Plasmon lasers at deep subwavelength scale, Nature (London) **461**, 629 (2009).
[8] Y.-J. Lu, J. Kim, H.-Y. Chen, C. Wu, N. Dabidian, C. E. Sanders, C.-Y. Wang, M.-Y. Lu, B.-H. Li, X. Qiu, W.-H. Chang, L.-J. Chen, G. Shvets, C.-K. Shih, and S. Gwo, Plasmonic nanolaser using epitaxially grown silver film, Science **337**, 450 (2012).
[9] R.-M. Ma, R. F. Oulton, V. J. Sorger, and X. Zhang, Plasmon lasers: Coherent light source at molecular scales, Laser Photonics Rev. **7**, 1 (2013).
[10] H. Wu, Y. X. Gao, P. Z. Xu, X. Guo, P. Wang, D. X. Dai, and L. M. Tong, Plasmonic nanolasers: Pursuing extreme lasing conditions on nanoscale, Adv. Opt. Mater. **7**, 1900334 (2019).
[11] S. I. Azzam, A. V. Kildishev, R.-M. Ma, C.-Z. Ning, R. Oulton, V. M. Shalaev, M. I. Stockman, J.-L. Xu, and X. Zhang, Ten years of spasers and plasmonic nanolasers, Light **9**, 90 (2020).
[12] L. Landau, On the vibrations of the electronic plasma, Zh. Eksp. Teor. Fiz. **16**, 574 (1946).
[13] G. Kewes, K. Herrmann, R. Rodríguez-Oliveros, A. Kuhlicke, O. Benson, and K. Busch, Limitations of Particle-Based Spasers, Phys. Rev. Lett. **118**, 237402 (2017).
[14] J. D. Jackson, *Classical Electrodynamics*, 3rd ed. (Wiley, New York, 1998).
[15] V. R. Almeida, Q. F. Xu, C. A. Barrios, and M. Lipson, Guiding and confining light in void nanostructure, Opt. Lett. **29**, 1209 (2004).
[16] Q. Xu, V. R. Almeida, R. R. Panepucci, and M. Lipson, Experimental demonstration of guiding and confining light in nanometer-size low-refractive-index material, Opt. Lett. **29**, 1626 (2004).
[17] Q. Lu, F.-J. Shu, and C.-L. Zou, Dielectric bow-tie nanocavity, Opt. Lett. **38**, 5311 (2013).
[18] S. Hu and S. M. Weiss, Design of photonic crystal cavities for extreme light concentration, ACS Photonics **3**, 1647 (2016).
[19] H. Choi, M. Heuck, and D. Englund, Self-Similar Nanocavity Design with Ultrasmall Mode Volume for Single-Photon Nonlinearities, Phys. Rev. Lett. **118**, 223605 (2017).

[20] S. Hu, M. Khater, R. Salas-Montiel, E. Kratschmer, S. Engelmann, W. M. J. Green, and S. M. Weiss, Experimental realization of deep-subwavelength confinement in dielectric optical resonators, Sci. Adv. **4**, eaat2355 (2018).
[21] See Supplemental Material at http://link.aps.org/supplemental/10.1103/PhysRevLett.129.013902 for details of CNP preparation, numerical calculation and discussion of mode properties and lasing threshold, and experimental characterization, which includes Refs. [22–35].
[22] Z.-Z. Li, L. Wang, H. Fan, Y.-H. Yu, Q.-D. Chen, S. Juodkazis, and H.-B. Sun, O-FIB: Far-field-induced near-field breakdown for direct nanowriting in an atmospheric environment, Light **9**, 41 (2020).
[23] H. Blom and H. Brismar, STED microscopy: Increased resolution for medical research?, J. Intern. Med. **276**, 560 (2014).
[24] S. Mokhov, R. El-Ganainy, and D. N. Christodoulides, Power circulation via negative energy-flux wormholes in optical nanowaveguides, Opt. Express **14**, 3255 (2006).
[25] A. V. Maslov and C. Z. Ning, Reflection of guided modes in a semiconductor nanowire laser, Appl. Phys. Lett. **83**, 1237 (2003).
[26] S. Wang, Z. Hu, H. Yu, W. Fang, M. Qiu, and L. Tong, Endface reflectivities of optical nanowires, Opt. Express **17**, 10881 (2009).
[27] W. Heisenberg, Über den anschaulichen Inhalt der quantentheoretischen Kinematik und Mechanik, Z. Phys. **43**, 172 (1927).
[28] I. Bialynicki-Birula and Z. Bialynicka-Birula, Heisenberg uncertainty relations for photons, Phys. Rev. A **86**, 022118 (2012).
[29] I. Bialynicki-Birula and Z. Bialynicka-Birula, Uncertainty Relation for Photons, Phys. Rev. Lett. **108**, 140401 (2012).
[30] M. Kanezashi, A. Yamamoto, T. Yoshioka, and T. Tsuru, Characteristics of ammonia permeation through porous silica membranes, AIChE J. **56**, 1204 (2010).
[31] D. Minoli, *Nanotechnology Applications to Telecommunications and Networking*, 1st ed. (Wiley, New York, 2005).
[32] A. K. Wright and M. R. Thompson, Hydrodynamic structure of bovine serum albumin determined by transient electric birefringence, Biophys. J. **15**, 137 (1975).
[33] M. Barcena, G. T. Oostergetel, W. Bartelink, F. G. A. Faas, A. Verkleij, P. J. M. Rottier, A. J. Koster, and B. J. Bosch, Cryo-electron tomography of mouse hepatitis virus: Insights into the structure of the coronavirion, Proc. Natl. Acad. Sci. U.S.A. **106**, 582 (2009).
[34] Y. Xiao, C. Meng, P. Wang, Y. Ye, H. Yu, S. Wang, F. Gu, L. Dai, and L. Tong, Single-nanowire single-mode laser, Nano Lett. **11**, 1122 (2011).
[35] L. M. Tong, J. Y. Lou, R. R. Gattass, S. L. He, X. W. Chen, L. Liu, and E. Mazur, Assembly of silica nanowires on silica aerogels for microphotonic devices, Nano Lett. **5**, 259 (2005).
[36] S. Ninomiya and S. Adachi, Optical properties of cubic and hexagonal CdSe, J. Appl. Phys. **78**, 4681 (1995).
[37] Y. Yang, D. Zhu, W. Yan, A. Agarwal, M. Zheng, J. D. Joannopoulos, P. Lalanne, T. Christensen, K. K. Berggren, and M. Soljačić, A general theoretical and experimental framework for nanoscale electromagnetism, Nature (London) **576**, 248 (2019).
[38] Y. Ding, Q. Yang, X. Guo, S. S. Wang, F. X. Gu, J. Fu, Q. Wan, J. P. Cheng, and L. M. Tong, Nanowires/microfiber hybrid structure multicolor laser, Opt. Express **17**, 21813 (2009).
[39] Y. G. Ma, X. Guo, X. Q. Wu, L. Dai, and L. M. Tong, Semiconductor nanowire lasers, Adv. Opt. Photonics **5**, 216 (2013).
[40] H. Chen, S. Wang, and R.-M. Ma, Characterization of plasmonic nanolasers in spatial, momentum, and frequency spaces, IEEE J. Quantum Electron. **54**, 1 (2018).
[41] C. Z. Ning, Semiconductor nanolasers, Phys. Status Solidi (b) **247**, 774 (2010).
[42] M. A. Zimmler, F. Capasso, S. Müller, and C. Ronning, Optically pumped nanowire lasers: Invited review, Semicond. Sci. Technol. **25**, 024001 (2010).
[43] H. A. Bethe, Theory of diffraction by small holes, Phys. Rev. **66**, 163 (1944).
[44] U. Dürig, D. W. Pohl, and F. Rohner, Near-field optical-scanning microscopy, J. Appl. Phys. **59**, 3318 (1986).
[45] T. W. Ebbesen, H. J. Lezec, H. F. Ghaemi, T. Thio, and P. A. Wolff, Extraordinary optical transmission through sub-wavelength hole arrays, Nature (London) **391**, 667 (1998).
[46] Y. N. Xia, P. D. Yang, Y. G. Sun, Y. Y. Wu, B. Mayers, B. Gates, Y. D. Yin, F. Kim, and H. Q. Yan, One-dimensional nanostructures: Synthesis, characterization, and applications, Adv. Mater. **15**, 353 (2003).
[47] M. Law, D. J. Sirbuly, J. C. Johnson, J. Goldberger, R. J. Saykally, and P. Yang, Nanoribbon waveguides for subwavelength photonics integration, Science **305**, 1269 (2004).
[48] K. Shaklee, R. Nahory, and R. Leheny, Optical gain in semiconductors, J. Lumin. **7**, 284 (1973).
[49] S. Geburt, A. Thielmann, R. Röder, C. Borschel, A. McDonnell, M. Kozlik, J. Kühnel, K. A. Sunter, F. Capasso, and C. Ronning, Low threshold room-temperature lasing of CdS nanowires, Nanotechnology **23**, 365204 (2012).
[50] S. H. Pan, S. S. Deka, A. El Amili, Q. Gu, and Y. Fainman, Nanolasers: Second-order intensity correlation, direct modulation and electromagnetic isolation in array architectures, Prog. Quantum Electron. **59**, 1 (2018).
[51] S. H. Pan, Q. Gu, A. E. Amili, F. Vallini, and Y. Fainman, Dynamic hysteresis in a coherent high-β nanolaser, Optica **3**, 1260 (2016).
[52] B. Yang, G. Chen, A. Ghafoor, Y. Zhang, Y. Zhang, Y. Zhang, Y. Luo, J. Yang, V. Sandoghdar, J. Aizpurua, Z. Dong, and J. G. Hou, Sub-nanometre resolution in single-molecule photoluminescence imaging, Nat. Photonics **14**, 693 (2020).
[53] J. Weiner, V. S. Bagnato, S. Zilio, and P. S. Julienne, Experiments and theory in cold and ultracold collisions, Rev. Mod. Phys. **71**, 1 (1999).
[54] W. Zhu, R. Esteban, A. G. Borisov, J. J. Baumberg, P. Nordlander, H. J. Lezec, J. Aizpurua, and K. B. Crozier, Quantum mechanical effects in plasmonic structures with subnanometre gaps, Nat. Commun. **7**, 11495 (2016).